Computers and Geotechnics 39 (2012) 8–16

Contents lists available at SciVerse ScienceDirect

Computers and Geotechnics

journal homepage: www.elsevier.com/locate/compgeo

Numerical analysis of the failure process around a circular opening in rock

S.Y. Wang [a,*], S.W. Sloan [a], D.C. Sheng [a], C.A. Tang [b]

[a] Centre for Geotechnical and Materials Modelling, Civil, Surveying and Environmental Engineering, The University of Newcastle, Callaghan, NSW 2308, Australia
[b] School of Civil & Hydraulic Engineering, Dalian University of Technology, Dalian 116024, PR China

ARTICLE INFO

Article history:
Received 12 May 2011
Received in revised form 24 July 2011
Accepted 8 August 2011

Keywords:
Heterogeneity
Acoustic emission
Underground opening
Finite element method
Failure process

ABSTRACT

Damage and fracture propagation around underground excavations are important issues in rock engineering. The analysis of quasi-brittle materials can be performed using constitutive laws based upon damage mechanics. The finite element code RFPA2D (Rock Failure Process Analysis) based on damage mechanics was used to simulate a loading-type failure process around an underground excavation (model tunnel) in brittle rock. One of the features of RFPA2D is the capability of modeling heterogeneous materials. In the current model, the effect of the homogeneous index (m) of rock on the failure modes of a model tunnel in rock was studied. In addition, by recording the number of damaged elements and the associated amount of energy released, RFPA2D is able to simulate acoustic activities around circular openings in rock. The results of a numerical simulation of a model tunnel were in very good agreement with the experimental test using the acoustic emission technique. Finally, the influence of the lateral confining pressure on the failure mechanism of the rock around the model tunnel was also investigated by numerical simulations.

1. Introduction

Damage and fracture propagation around underground excavations are important issues in rock engineering. It is generally recognized that, for a circular opening in a brittle rock subjected to different stress fields, there exist three different fracture types: spalling fracture under a compressive stress field, the primary fracture under a tensile stress field, and remote fracture under a mixture of compressive and tensile stress fields [1]. Lajtai et al. [2,3] conducted biaxial compression tests at the laboratory scale to observe the development of fracture patterns and reported the fracture phenomena. In addition, Fakhimi et al. [4] performed a biaxial compression test on a sandstone specimen with a circular opening to simulate the failure around an underground excavation in brittle rock. The axial force and displacements were monitored throughout the failure process, and micro-cracking was detected by the acoustic emission technique.

In addition, to reflect the effect of cracks on the mechanical properties of a rock mass, many theoretical models [5,6] have been proposed based on fracture mechanics. However, for fracture mechanics models, like other classical mathematical models, it is difficult to characterize the entire fracture process, which involves the initiation, propagation, and coalescence of micro-cracks through to the formation of a full-scale macro-crack in the host rock. Therefore, numerical modeling may be used to capture the detail of the processes involved in progressive fracture. For example, the distinct element computer program, particle flow code (PFC2D) was used to simulate the damage zone around the circular opening observed in the laboratory test [4]. These numerically simulated results showed that the crack pattern and the spalling of the opening matched the laboratory results well. Wang et al. [7] used the finite element method (FEM) to study the effect of heterogeneity and anisotropy of rock in the excavation damaged zone around circular excavations in granite. The micro-crack pattern in the numerical model was consistent with the locations of acoustic emission (AE) determined in the laboratory test.

The aim of the study reported here is to examine the progressive failure leading to collapse around a circular opening in brittle heterogeneous rock, which is subjected to different confining pressures. For this purpose, a numerical tool, Rock Failure Process Analysis code, RFPA (Rock Failure Process Analysis) [8], was used. The program is able to capture the heterogeneity of rock at the meso-level using a probabilistic variation of the mechanical properties of the materials [9]. The variations of properties, such as the elastic modulus and the strength, were assigned in the finite element model to conform to a Weibull probability distribution. RFPA has been used extensively to simulate the failure process of rocks [10–17]. The unique feature of this code is that no a priori assumptions need to be made about where and how fracture and failure will occur: cracking can occur spontaneously and can exhibit a variety of mechanisms when certain local stress conditions are exceeded.

* Corresponding author.
E-mail addresses: Shanyong.Wang@newcastle.edu.au (S.Y. Wang), Scott.Sloan@newcastle.edu.au (S.W. Sloan), Daichao.Sheng@newcastle.edu.au (D.C. Sheng), catang@mechsoft.cn (C.A. Tang).

0266-352X/$ - see front matter Crown Copyright © 2011 Published by Elsevier Ltd. All rights reserved.
doi:10.1016/j.compgeo.2011.08.004

2. Numerical model descriptions and setup

Briefly, the code RFPA2D [11] is a two-dimensional finite element code that can simulate the fracture and failure process of quasi-brittle materials such as rock. To model the failure of rock material (or rock mass), the rock medium is assumed to be composed of many meso-scopic rectangular elements of the same size. Their material properties differ and are specified according to a Weibull distribution [18,19]. These elements act as the four-nodded iso-parametric elements for finite element analysis. Elastic damage mechanics is used to describe the constitutive law of the meso-scale elements, and the maximum tensile strain criterion and the Mohr–Coulomb criterion are utilized as damage thresholds [17,19].

2.1. Meso-scale modeling with elastic damage mechanics

In the proposed model, the elastic damage mechanics approach is employed to model the mechanical behavior of meso-scale elements. For each element, the material is assumed to be linear elastic, isotropic and damage-free before loading, with its elastic properties defined by the elastic modulus and Poisson's ratio. After the initiation of damage, based on elastic damage mechanics, the strength and stiffness of the element is assumed to degrade gradually as damage progresses, with the elastic modulus of the damaged material given by [7,19]

$$E = (1-\omega)E_0 \tag{1}$$

where ω represents the damage variable. The parameters E and E_0 are elastic modulus of the damaged and the undamaged material, respectively.

The constitutive relationship of meso-scopic element under uniaxial tension is expressed as [17]

$$\omega = \begin{cases} 0 & \varepsilon > \varepsilon_{t0} \\ 1-\frac{f_{tr}}{E_0\varepsilon} & \varepsilon_{tu} < \varepsilon \leqslant \varepsilon_{t0} \\ 1 & \varepsilon \leqslant \varepsilon_{tu} \end{cases} \tag{2}$$

where f_{tr} is the residual tensile strength, which is given as $f_{tr} = \lambda f_{t0} = \lambda E_0 \varepsilon_{t0}$. The parameters f_{t0} and λ are uniaxial tensile strength and residual strength coefficient, respectively, and ε_{t0} is the strain at the elastic limit, which can be called the threshold strain. ε_{tu} is the ultimate tensile strain of element, at which the element would be completely damaged. The ultimate tensile strain is defined as $\varepsilon_{tu} = \eta\varepsilon_{t0}$, where η is called the ultimate strain coefficient. Eq. (2) can be expressed as [19]

$$\omega = \begin{cases} 0 & \varepsilon > \varepsilon_{t0} \\ 1-\frac{\lambda\varepsilon_{t0}}{\varepsilon} & \varepsilon_{tu} < \varepsilon \leqslant \varepsilon_{t0} \\ 1 & \varepsilon \leqslant \varepsilon_{tu} \end{cases} \tag{3}$$

It is noted that the sign convention used throughout this paper is that tensile stress and strain are positive. In addition, it is assumed that the damage to a meso-scopic element in multiaxial stress conditions is also isotropic and elastic [8]. Under multiaxial stress states, the element is still damaged in tensile mode when the equivalent major tensile strain $\bar{\varepsilon}$ reaches the threshold strain ε_{t0}. The equivalent principal strain $\bar{\varepsilon}$ is defined as follows [17,19]:

$$\bar{\varepsilon} = -\sqrt{\langle-\varepsilon_1\rangle^2 + \langle-\varepsilon_2\rangle^2 + \langle-\varepsilon_3\rangle^2} \tag{4}$$

where ε_1, ε_2 and ε_3 are three principal strains, and $\langle\cdot\rangle$ is a function defined as follows: [17]

$$\langle x\rangle = \begin{cases} x & x \geqslant 0 \\ 0 & x < 0 \end{cases} \tag{5}$$

The constitutive law for an element subjected to multiaxial stresses can be easily obtained by substituting the strain ε in Eqs. (2) and (3) with the equivalent strain $\bar{\varepsilon}$. The damage variable is expressed as [17,20]

$$\omega = \begin{cases} 0 & \bar{\varepsilon} > \varepsilon_{t0} \\ 1-\frac{\lambda\varepsilon_{t0}}{\bar{\varepsilon}} & \varepsilon_{tu} < \bar{\varepsilon} \leqslant \varepsilon_{t0} \\ 1 & \bar{\varepsilon} \leqslant \varepsilon_{tu} \end{cases} \tag{6}$$

To study the damage to the element when it is under compressive and shear stress, the Mohr–Coulomb criterion, expressed as follows, is chosen to be the second damage threshold [13–15].

$$F = \sigma_1 - \frac{1+\sin\varphi}{1-\sin\varphi}\sigma_3 \geqslant f_{c0} \tag{7}$$

where σ_1 and σ_3 are major and minor principal stresses, respectively. f_{c0} is the uniaxial compressive strength, and φ is the internal friction angle of the meso-scopic element. This kind of damage is called shear damage because the damage occurs when the stress conditions of the element meet the Mohr–Coulomb criterion. Similarly, when the element is under uniaxial compression and damaged according to the Mohr–Coulomb criterion, the expression for the damage variable ω can be described as follows [7,19].

$$\omega = \begin{cases} 0 & \varepsilon < \varepsilon_{c0} \\ 1-\frac{\lambda\varepsilon_{c0}}{\varepsilon} & \varepsilon \geqslant \varepsilon_{c0} \end{cases} \tag{8}$$

where λ is also residual strength coefficient and λ is equal to f_{cr}/f_{c0} or f_{tr}/f_{t0} when the element is under uniaxial compression or tension. Previous work with the code [19] has shown that, provided the residual strength coefficient λ is in the range $0 < \lambda \leqslant 0.1$, the effect of constitutive parameters on the failure evolution is minor. Therefore, when RFPA2D is used to study the brittle failure of rock, these two parameters must be specified within their respective ranges.

When an element is under a multi-axial stress state and its strength satisfies the Mohr–Coulomb criterion, damage occurs, and the effect of other principal stresses in this model during the damage evolution process should be considered. When the Mohr–Coulomb criterion is met, the maximum principal strain (maximum compressive principal strain) ε_{c0} is calculated at the peak value of the maximum principal stress (maximum compressive principal stress) [19].

$$\varepsilon_{c0} = \frac{1}{E_0}\left[f_{c0} + \frac{1+\sin\varphi}{1-\sin\varphi}\sigma_3 - \mu(\sigma_1+\sigma_2)\right] \tag{9}$$

where μ is Poisson's ratio. In this respect, the shear damage evolution is only related to the maximum compressive principal strain ε_1. The maximum compressive principal strain ε_1 of the damaged element will substitute for the uniaxial compressive strain in Eq. (8). Thus, Eq. (8) can be extended to triaxial stress states for shear damage [7,19].

$$\omega = \begin{cases} 0 & \varepsilon_1 < \varepsilon_{c0} \\ 1-\frac{\lambda\varepsilon_{c0}}{\varepsilon_1} & \varepsilon_1 \geqslant \varepsilon_{c0} \end{cases} \tag{10}$$

In RFPA2D, the specified displacement (or load) is applied on the specimen step by step. If some elements are damaged at this step, according to the derivation of the damage variable ω and Eq. (1), the damaged elastic modulus of the elements at each stress or strain level can be calculated when their stresses or strains meet one of the two damage thresholds. Then, the calculation must be

restarted under the current boundary and loading conditions to find the stress redistribution in the specimen until no new damage occurs. Finally, the applied load (or displacement) is increased and goes into the analysis of the next step. By this means, the progressive failure process of rock subjected to gradually increasing static loading can be simulated. A user-friendly pre- and post-processor is integrated into RFPA2D to prepare the input data and display the numerical results [8–10].

In addition, in RFPA2D, the failure (or damage) of every element is assumed to be a source of acoustic events because the failed element must release its elastic energy stored during the deformation. Therefore, by recording the number of damaged elements and associated amount of energy release, RFPA2D is capable of simulating the AE activities [10]. According to Tang and Kaiser [8], the cumulative damage, D, can be calculated by the following Eq. (11).

$$D = \frac{1}{N}\sum_{i=1}^{s} n_i \tag{11}$$

where s is the number of calculation steps, n_i is the number of damaged elements in the ith step and N is the total number of elements in the model. In addition, when the element fails, the energy released is calculated by Eq. (12) [12].

$$W_i = \frac{1}{2E}(\sigma_1^2 + \sigma_3^2 - 2\mu\sigma_1\sigma_3)V \tag{12}$$

where i is the element number, W_i is the released elastic strain energy, E is the elastic modulus, σ_1 and σ_3 are the major and minor principle stresses, respectively, μ is the Poisson ratio, and V is the element volume [12]. By recording the counts of all failed elements and released energies when failure occurs, the AE phenomena associated with the progressive failure process can be simulated.

2.2. Model setup

In this paper, a plane strain (biaxial) test was performed on a rectangular prism of Berea sandstone. The specimen was machined with a 14 mm diameter hole to simulate an underground opening (Fig. 1), although failure was achieved through loading rather than excavation of the circular opening [4]. The model had dime nsions of 40 mm × 100 mm. The mesh for the model had 12 0 × 300 = 36,000 elements. In RFPA2D, the rock is assumed to be composed of many meso-scopic elements of the same size, and the mechanical properties of these elements are assumed to conform to a given Weibull distribution [18].

$$f(u) = \frac{m}{u_0}\left(\frac{u}{u_0}\right)\exp\left(-\frac{u}{u_0}\right)^m \tag{13}$$

where u is the mechanical parameter (Young's modulus or strength) of the elements and the parameter m defines the shape of the distribution function. From the properties of the Weibull distribution, a larger value of m implies a more homogeneous material and vice versa. Therefore, the parameter m is called the homogeneity index in RFPA2D. For higher values of the homogeneity index, the Young's modulus and strengths of more of the elements are concentrated closer to u_0. In the current study, to investigate the effect of the heterogeneity of rock on the failure mechanism of a model tunnel, different homogeneity indexes of 1.1, 3, 5, 7 and 10 were selected. In addition, different confining pressures of 3, 5, 7, 9 and 11 were applied to study the failure behavior of the circular opening in rock. All of the input parameters in the numerical model are listed in Table 1. To calibrate the numerical model of RFPA, the boundary conditions and input parameters of the rock were the same as those in the laboratory tests and the numerical model of PFC [4].

The failure approach is adopted in RFPA2D, where meso-scopic fracturing occurs when the stress of an element satisfies a strength criterion [8,9]. In confined conditions, the loading technique increased the vertical and horizontal loads simultaneously to the level of the constant confining stress and then increased vertical load (displacement control) until the model collapsed. The stress and deformation were computed in each element. The specified displacement is applied to the specimen step by step. At steps in which the stress in some elements satisfies the strength criterion, the element is damaged either in shear or in tension and becomes weak according to the rules specified in the literature [8–10]. The stress and deformation distribution throughout the sample are then adjusted instantaneously after each element rupture to reach the equilibrium state. At positions with increased stress due to stress redistribution, the stress may exceed the critical value and further ruptures are caused. The process is repeated until no failure elements are present. Greater external displacement is then applied. Energy is stored in the elements during the loading process and is released as acoustic emissions through the onset of element failures. Due to the stress redistribution and the deformation induced interactions, a single element failure may induce an avalanche of additional failures in neighboring elements, leading to a chain reaction that releases more energy.

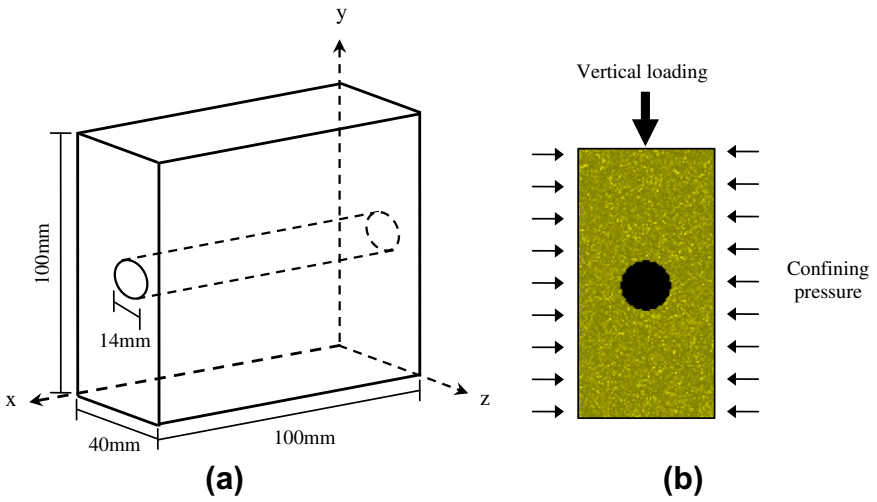

Fig. 1. Model setup: (a) specimen geometry [4] and (b) loading configuration.

Table 1
Material properties of specimens [4].

Parameter	Value
Homogeneity index (m)	1.1, 3, 5, 7, 10
Mean compressive strength (σ_0)	40 MPa
Mean Young's modulus (E_0)	16,000 MPa
Tension cut-off	10%
Friction angle (φ)	30
Confining pressure	3, 5, 7, 9, 11 MPa
Poisson ratio (υ)	0.28
Density	2600 kg/m^3

3. Numerical results and discussions

3.1. The evolution of cracks around a circular opening in rock

Fig. 2 shows the numerically simulated failure process around a circular opening in rock with $m = 2.0$ and a lateral confining pressure of 7.5 MPa. Fig. 3 shows the comparison of the laboratory test results (a) [4], the numerically simulated results according to PFC (b) [4], and the numerically simulated results according to RFPA (c). The Stages A–H in Fig. 2 correspond to the Points A–H in Fig. 4. Fig. 4 shows the numerically simulated result of normalized load (force/area) versus normalized displacement (displacement/height) of the specimens together with the AE events.

In Fig. 2, by following the crack generation in the specimen during the failure process, it was observed that the cracks start to develop from the periphery of the circular opening (Stage A), where the compressive stresses is highlighted. Stage A corresponds to the point A in Fig. 4, which indicates the yield point of the normalized load versus normalized displacement. With continued loading, more damage is developed (Stages B–E). During this period, some small cracks propagate and coalescence into larger cracks. In Fig. 4, the AE events increase in relation to the distinct stress drops in Stages A–E. With increased loading until Stage F, more micro-cracks localize near the lateral boundaries of the circular opening and form notches. However, even during the evolution of these notches, some cracks are formed near the eventual rupture zone.

With continued loading (Stage G), more damage is developed, and further cracks are generated close to the rupture zone on both sides of the specimen. Eventually, one of them prevails and continues to propagate. Finally, the specimen shows a macroscopic discontinuity along the rupture zone (Stage H). It is noted that, even in Stage H, there is still the residual strength of the circular opening in Fig. 4. The damage zone and micro-crack patterns in Fig. 3c are similar to those observed from the laboratory test in Fig. 3a and the numerically simulated results according to PFC in Fig. 3b [4]. In addition, the normalized load–displacement curve for this specimen in Fig. 4 can be compared with the results of the actual lab test in Fig. 5 [4]. Although the RFPA simulated specimen shows a slightly stiffer response, both the peak loads and the accumulated AE events match very well. In addition, by comparing the cracks evolution in the specimen during the failure process, it was observed that the cracks distribution is not symmetrical around the circular opening. One possible reason is due to the heterogeneity of the rock. In the next subsection, the influence of the heterogeneity of rock on crack patterns around a circular opening is reported.

3.2. Influence of the heterogeneity of rock on the failure mechanism of a circular opening in rock

In this section, to study the effect of the heterogeneity of rock on the failure mechanism of a model tunnel, different homogeneity indexes of 1.1, 3, 5, 7 and 10 were selected. This mechanism can be explained by examining the final stage of failure of the specimen (Fig. 6) and plots of the normalized load (force/area) versus normalized displacement (displacement/height) (Fig. 7) during the failure process of circular opening specimens. The confining

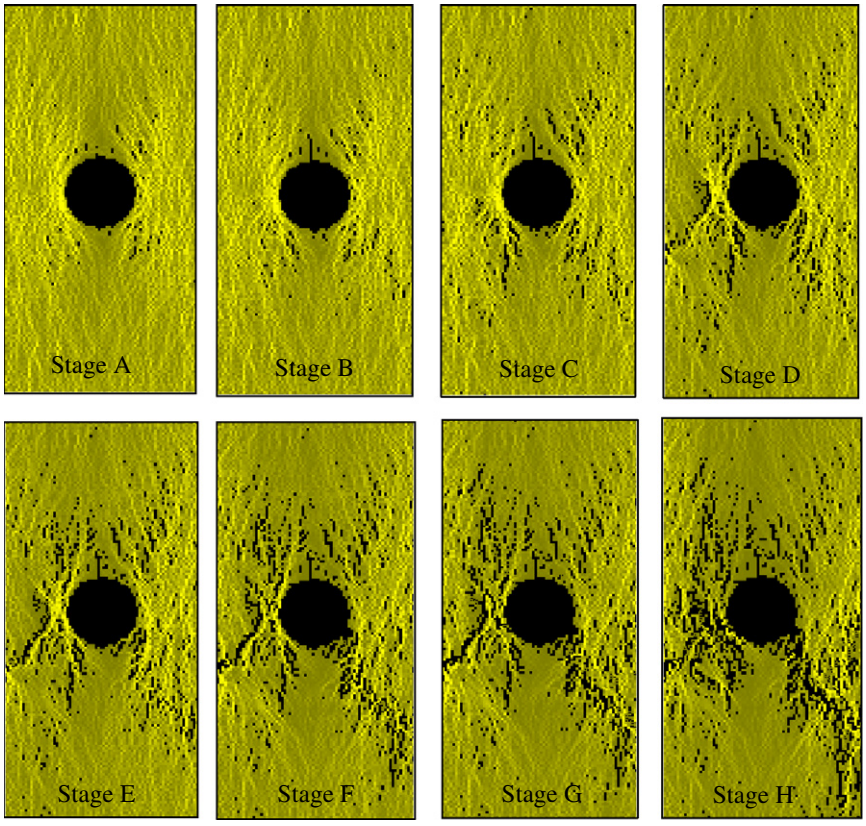

Fig. 2. Numerically simulated failure process around a circular opening in rock with $m = 2.0$ and a lateral confining pressure of 7.5 MPa (shear stress distribution).

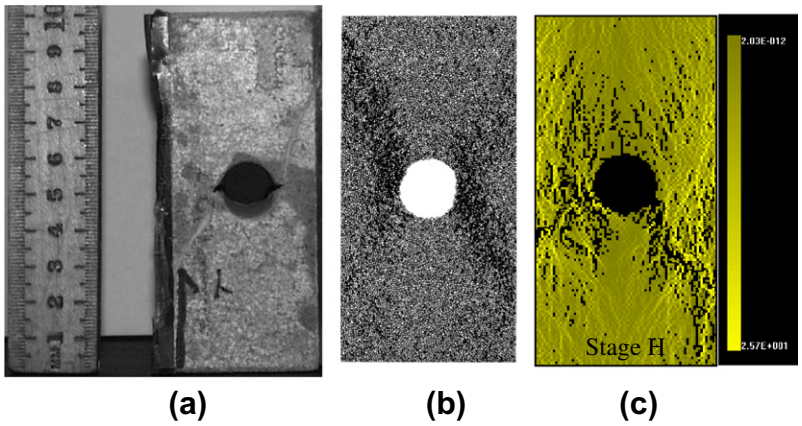

Fig. 3. (a) Comparison of laboratory test results [4]; (b) numerically simulated results by PFC [4]; and (c) numerically simulated results by RFPA2D.

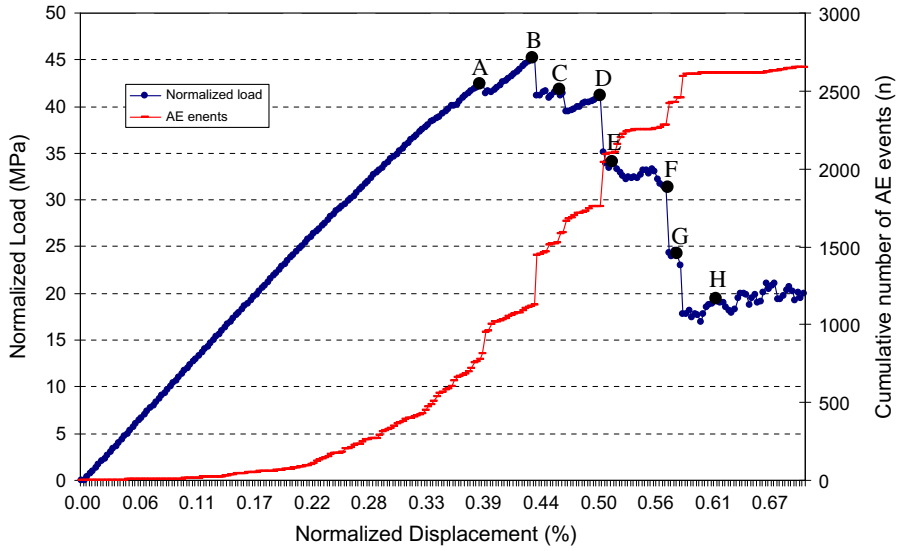

Fig. 4. Numerically simulated results of normalized load (force/area) versus normalized displacement (displacement/height) behavior of the specimen together with the AE events (RFPA2D), with $m = 2.0$ and a lateral confining pressure of 7.5 MPa.

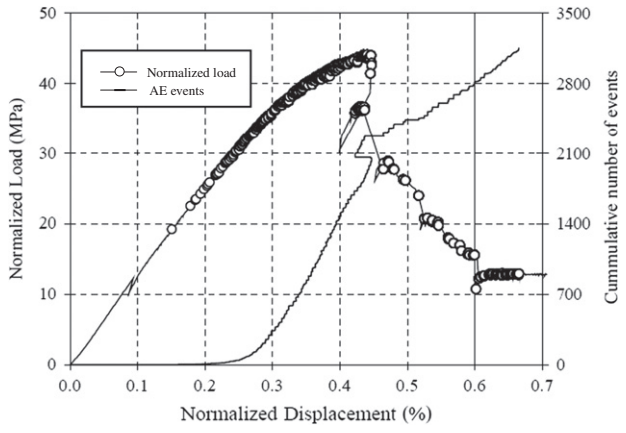

Fig. 5. Experimental results of normalized load (force/area) versus normalized displacement (displacement/height) behavior of the specimen together with the AE events [4].

pressure is 3 MPa. In Fig. 6, for the heterogeneous rock (e.g., $m = 1.1$), the micro-cracks are distributed around the circular opening, and the final main crack forms and extends from the notches on the periphery of circular opening in the vertical direction with a gradual incline toward the vertical boundaries. However, for the relatively homogeneous rock (e.g., $m = 3$ and 5), the number of micro-cracks decreases. Moreover, there is a main crack extending from the notch with a gradual incline to the downward vertical boundary, and another final main crack is more concentrated on the vertical direction. Furthermore, for the highly homogeneous rock (e.g., $m = 7$ and 10), the number of micro-cracks is much lower, and the final main crack almost propagates in the vertical direction ($m = 10$). The failure modes in Fig. 6 are different than those in Fig. 2 because the confining pressure is different. The effect of the confining pressure on the failure modes of a circular opening will be investigated in Section 3.3.

The complete curves of the normalized load (force/area) versus normalized displacement (displacement/height) simulated for the specimens are shown in Fig. 7. Obviously, the normalized load–displacement relation depends strongly on the heterogeneity of the specimens. It shows that the shape of the relatively heterogeneous rock (e.g., $m = 1.1$) has a gentler post-peak behavior under biaxial compression. Correspondingly, for increasingly homogeneous rocks with higher m, the shape tends to become increasingly sharper. In addition, the maximal normalized load (strength) of the specimens is closely related to the homogeneity index m. The

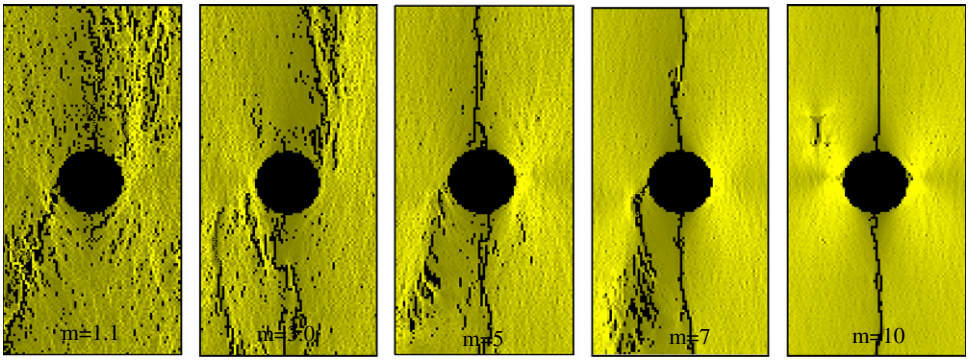

Fig. 6. Numerically simulated effect of the homogeneous index (m) of 1.1, 3, 5, 7, 10 on the failure modes of a circular opening with the same confining pressure of 3 MPa.

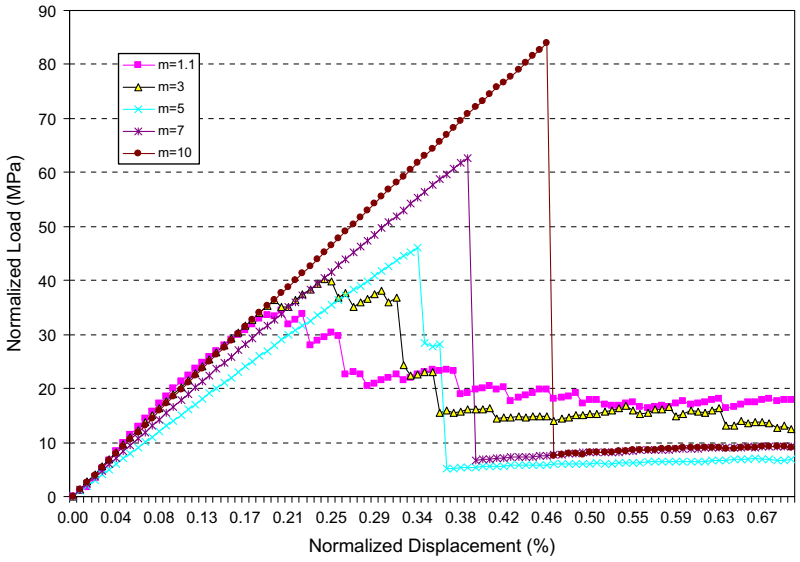

Fig. 7. Numerically simulated result of normalized load (force/area) versus normalized displacement (displacement/height) behavior of specimens with a homogeneous index of 1.1, 3, 5, 7 and 10 and the same confining pressure of 3 MPa.

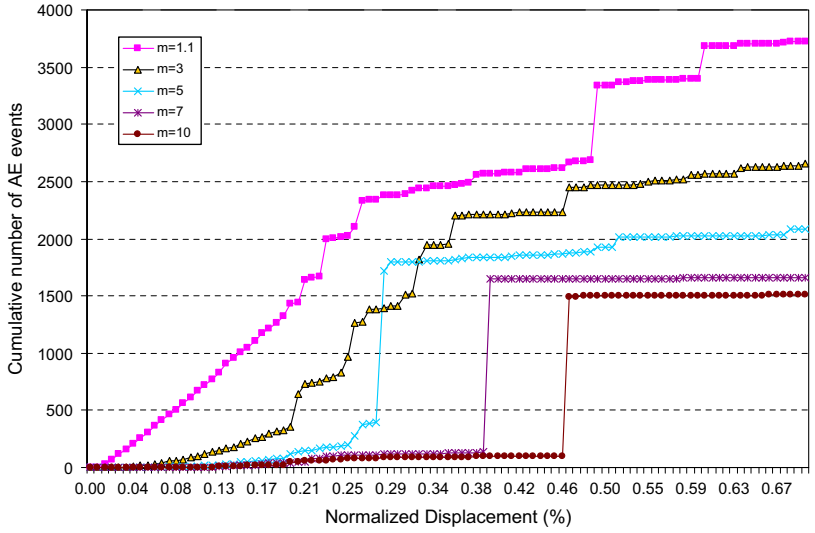

Fig. 8. Numerically simulated result of the cumulative number of AE events versus normalized displacement (displacement/height) of specimens with a homogeneous index of 1.1, 3, 5, 7 and 10 and the same confining pressure of 3 MPa.

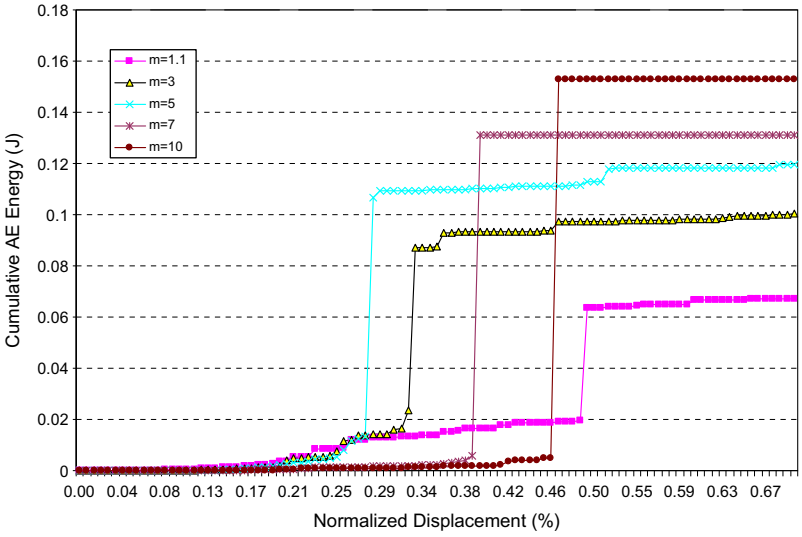

Fig. 9. Numerically simulated result of the cumulative AE energy versus normalized displacement (displacement/height) of specimens with a homogeneous index of 1.1, 3, 5, 7 and 10 and the same confining pressure of 3 MPa.

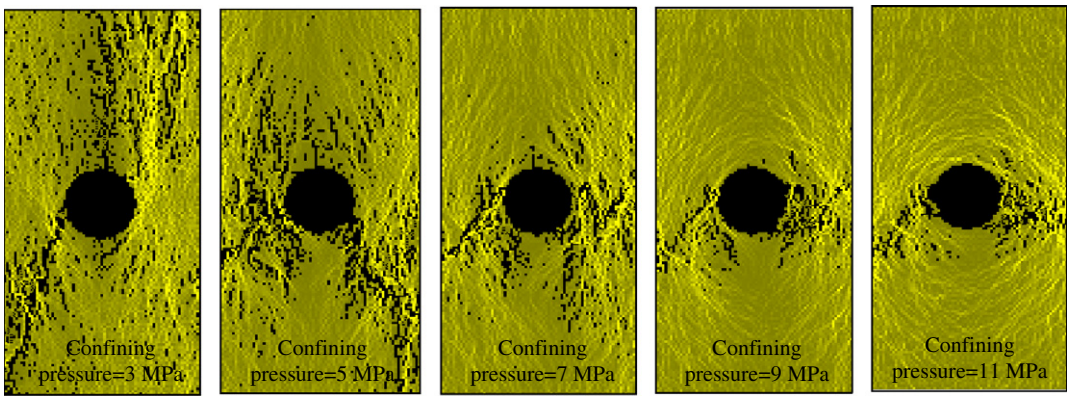

Fig. 10. Numerically simulated effect of a confining pressure of 3, 5, 7, 9, and 11 MPa on the failure modes of a circular opening ($m = 2$).

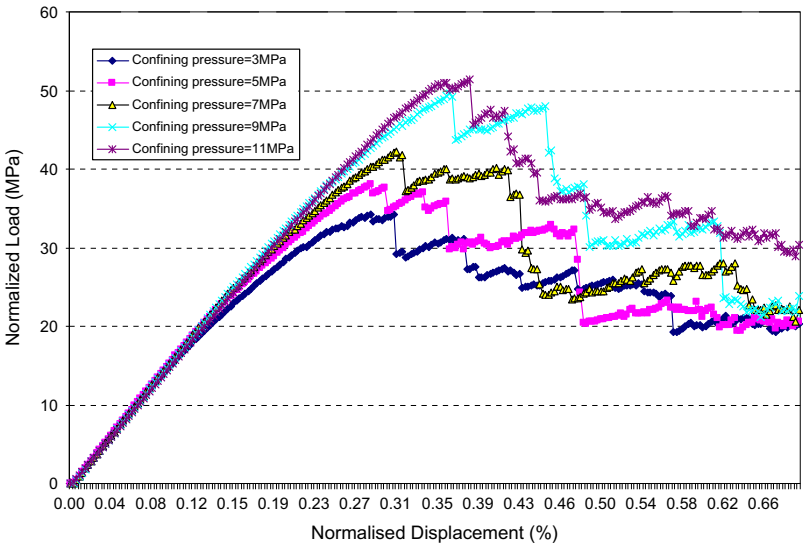

Fig. 11. Numerically simulated result of the normalized load (force/area) versus normalized displacement (displacement/height) of specimens with of confining pressures of 3, 5, 7, 9 and 11 MPa ($m = 2.0$).

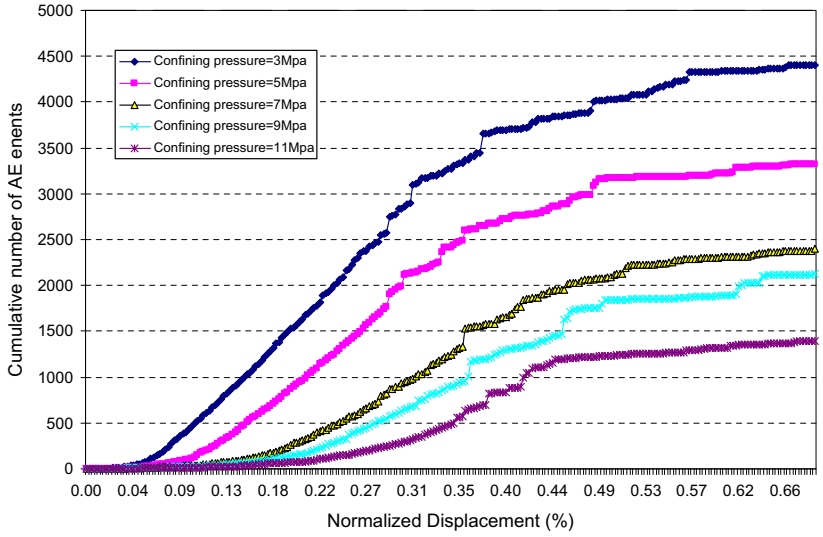

Fig. 12. Numerically simulated results of the cumulative number of AE events versus normalized displacement (displacement/height) of specimens with confining pressures of 3, 5, 7, 9 and 11 MPa (m = 2.0).

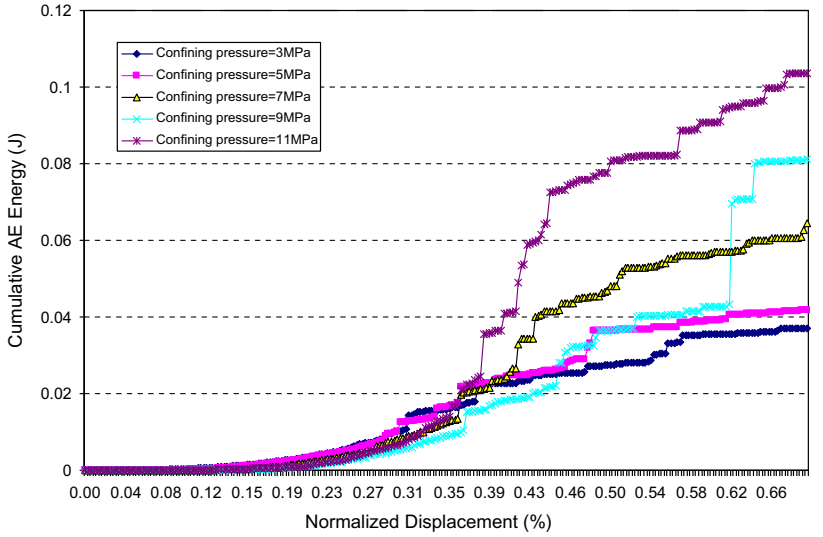

Fig. 13. Numerically simulated results of the cumulative AE energy versus normalized displacement (displacement/height) of specimens with confining pressures of 3, 5, 7, 9 and 11 MPa (m = 2.0).

higher the value of the homogeneity index m, the higher the strength of the specimen is. As a result, the curve becomes more linear, and the strength loss is also more precipitous.

In addition, Figs. 8 and 9 shows the numerically simulated result of the cumulative number of AE events and AE energy versus normalized displacement, respectively, when the homogeneous index (m) increases from 1.1 to 10. According to the Weibull distribution in Eq. (13), a larger value of m implies a more homogeneous material and vice versa. Under the same loading and boundary conditions, less damaged elements will occur in the more homogeneous material. Fig. 8 shows that the cumulative number of AE events decreases with increasing m value. For instance, when m = 1.1, the final cumulative number of AE events is 3665. When m is 3, 5, 7 and 10, the final cumulative number of AE events is 2633, 2137, 1723 and 1506, respectively.

However, with the increase of m, following the Weibull distribution, for higher values of m, the Young's modulus and strengths of more of the elements are concentrated closer to u_0. Thus, more elements with high Young's modulus and strength will be distributed in the rock mass with higher m, and the higher applied loads are needed to cause the damage of such elements. Accordingly, the damaged elements will release more elastic energy. It is the reason for the AE energy increase when m increases from 1.1 to 10 in Fig. 9. The above analysis also explains the increase of the normalized peak loads with the increase of m from 1.1 to 10 in Fig. 7.

3.3. Influence of confining pressures on the failure of a circular opening in rock

To study the effect of the confining pressure on the failure modes of a circular opening, different confining pressures of 3, 5, 7, 9 and 11 MPa were applied to the specimen. Fig. 10 shows the final failure stage of the specimen. In Fig. 10, for the low confining pressure of 3 MPa, the tensile cracks dominate in the failure process. For the immediate high confining pressures of 5 and 7 MPa, few tensile cracks of elements appear in the shear failure of specimens because the confining pressure restrains the initiation and propagation of tensile cracks. Moreover, for the high confining

pressures of 9 and 11 MPa, almost no tensile cracking occurs. Meanwhile, with increasing confining pressure, the micro-cracks concentrate gradually on the horizontal direction (i.e., the direction of the confining pressure). The V-shaped notch zones form in the end. During the formation of V-shaped notch zones, shear cracks plays a significant role in the formation of the crack patterns, with a wedge of failed material attempting to move laterally into the opening.

Fig. 11 shows the numerically simulated result of the normalized load (force/area) versus normalized displacement (displacement/height) of specimens with different confining pressures of 3, 5, 7, 9 and 11 MPa. From Fig. 11, the peak normalized load (strength) of the specimen increased with increasing confining pressure from 3 to 11 MPa. For instance, the peak normalized loads were 34.1, 37.9, 43.1, 50.2and 52.0 MPa with the confining pressures of 3, 5, 7, 9 and 11 MPa, respectively. Furthermore, Figs. 12 and 13 show the numerically simulated results of the cumulative number of AE events and AE energy versus normalized displacement, respectively, when the confining pressure increases from 3 to 11 MPa. In Fig. 12, the cumulative number of AE events decreases when the confining pressure increases from 3 to 11 MPa because the higher confining pressures restrain the initiation of tensile cracks and the propagation around the circular opening. To cause damage to the elements in the rock specimen, higher applied loads are needed. Accordingly, greater AE energy will be released during the process of failure of the rock specimen (see Fig. 13).

4. Conclusions

In this study, Rock Failure Process Analysis code (RFPA2D) was briefly introduced. The program is able to capture the heterogeneity of rock at the meso-level using a probabilistic variation of the mechanical properties of the materials. As a load is applied, the cracks will grow, interact and coalescence. The unique feature of this code is that no a priori assumptions are necessary about where and how cracks will occur. Tensile or shear cracks can be simulated when certain local stress conditions are exceeded. The numerically simulated results reproduced the development of cracks around a circular opening in rock, which were in very good agreement with the experimental results and numerical results by PFC [4]. Although the reality is often much more complex than the numerical models applied, the study provides interesting indications for improving the understanding of the mechanism of the failure of rock tunnels.

In addition, the numerically simulated results showed that the heterogeneity of rock plays an important role in the failure mechanism of the circular opening in rock. The higher the value of the homogeneity index m, the higher the strength of the specimen is. Accordingly, the curve becomes more linear, and the strength loss is also more precipitous. During the failure process of specimens, the cumulative number of AE events increases with increasing m, while the AE energy decreases.

Furthermore, according to the numerically simulated results, it is demonstrated that the confining pressure is another important factor that influences the failure mechanism of the circular opening in rock. For low confining pressures, the tensile cracks dominate the failure process; for higher confining pressures, shear cracks dominate the failure process because the confining pressure restrains the initiation and propagation of tensile cracks. As a result, the cumulative number of AE events decreases with higher confining pressure, while the AE energy increases with increasing confining pressure.

Acknowledgement

The work described in this paper was partially supported by Australian Research Council Grant DP0881238, to which the authors are very grateful.

References

[1] Hoek E. Rock fracture under static stress conditions. CSIR report MEG 383. National Mechanical Engineering Research Institute, Council for Scientific and Industrial Research, Pretoria, South Africa, 1965.
[2] Lajtai EZ, Lajtai VN. The collapse of cavities. Int J Rock Mech Min Sci 1975;12:81–6.
[3] Lajtai EZ, Carter BG, Duncan EJS. En echelon crack-arrays in potash salt rock. Rock Mech Rock Eng 1994;27(2):89–111.
[4] Fakhimi A, Carvalho F, Ishida T, Labuz JF. Simulation of failure around a circular opening in rock. Int J Rock Mech Min Sci 2002;39:507–15.
[5] Tokar G. Experimental analysis of the elasto-plastic zone surrounding a borehole in a specimen of rock-like material under multiaxial pressure. Eng Fract Mech 1990;35(4/5):879–87.
[6] Shao JF, Kondo D, Ikogou S. Stress-induced microcracking in rock and its influence on well bore stability analysis. Int J Rock Mech Min Sci Geomech Abstr 1994;31:149–55.
[7] Wang SH, Lee CI, Ranjith PG, Tang CA. Modeling the effects of heterogeneity and anisotropy on the excavation damaged/disturbed zone (EDZ). Rock Mech Rock Eng 2009;42:229–58.
[8] Tang CA, Kaiser PK. Numerical simulation of cumulative damage and seismic energy release during brittle rock failure – Part I: fundamentals. Int J Rock Mech Min Sci 1998;35(2):113–21.
[9] Tang CA, Liu H, Lee PKK, Tsui Y, Tham LG. Numerical tests on micro-macro relationship of rock failure under uniaxial compression, Part I: effect of heterogeneity. Int J Rock Mech Min Sci 2000;37(4):555–69.
[10] Tang CA. Numerical simulation of progressive rock failure and associated seismicity. Int J Rock Mech Min Sci 1997;34:249–61.
[11] Tang CA. A new approach to numerical method of modelling geological processes and rock engineering problems. Eng Geol 1998;49:207–14.
[12] Tang CA, Tham LG, Wang SH, Liu H, Li WH. A numerical study of the influence of heterogeneity on the strength characterization of rock under uniaxial tension. Mech Mater 2007;39:326–39.
[13] Wang SY, Lam KC, Au SK, Tang CA. Analytical and numerical study on the pillar rockburst mechanism. Rock Mech Rock Eng 2006;39:445–67.
[14] Wang SY, Sun L, Au ASK, Yang TH, Tang CA. 2D-numerical analysis of hydraulic fracturing in heterogeneous geo-materials. Construct Build Mater 2009;23(6):2196–206.
[15] Wang SY, Sloan SW, Huang ML, Tang CA. Numerical study of failure mechanism of serial and parallel rock pillars. Rock Mech Rock Eng 2011;44(2):179–98.
[16] Wang SY, Sloan SW, Liu HY, Tang CA. Numerical simulation of the rock fragmentation process induced by two drill bits subjected to static and dynamic loading. Rock Mech Rock Eng 2010;44(3):317–32.
[17] Zhu WC, Liu J, Tang CA, Zhao XD, Brady BH. Simulation of progressive fracturing processes around underground excavations under biaxial compression. Tunn Undergr Space Technol 2005;20(3):231–47.
[18] Weibull W. A statistical distribution function of wide applicability. J Appl Mech 1951;18:293–7.
[19] Zhu WC, Tang CA. Micromechanical model for simulating the fracture process of rock. Rock Mech Rock Eng 2004;37(1):25–56.
[20] Tang CA, Liang ZZ, Zhang YB, et al. Fracture spacing in layered materials: a new explanation based on two-dimensional failure process modeling. Am J Sci 2008;30(1):49–72.